

Speed Skating Modeling

A.L. Schwab, D.M. Fintelman, and O. den Braver

Abstract Advice about the optimal coordination pattern for an individual speed skater to reach their optimal performance, could well be addressed by simulation and optimization of a biomechanical model of speed skating. But before getting to this optimization approach one needs a model that matches observed behavior. In this chapter we present a simple 2-dimensional model of speed skating on the straights which mimics observed kinematic and force data. The primary features of the model are: the skater is modeled as three point masses, only motions in the horizontal plane are considered, air drag forces which are quadratic in the velocity and coulomb type ice friction forces at the skates are included, and idealized contact of the skate on the ice is modeled by a holonomic constraint in the vertical direction and a non-holonomic constraint in the lateral direction. Using the measured leg extension (relative motions of the skates with respect to the upper body) we are able to predict reasonable well the speed skater motions, even if we do not fit for that. The model seems to have the key terms for investigations of speed skating.

1 Introduction

The coordination pattern of speed skating appears to be completely different from all other types of human propulsion. In most patterns of human locomotion, humans generate forces by pushing against the environment in the opposite desired direction

A.L. Schwab (✉)

Laboratory for Engineering Mechanics, Delft University of Technology, Mekelweg 2,
2628 CD Delft, The Netherlands
e-mail: a.l.schwab@tudelft.nl

D.M. Fintelman

School of Sport and Exercise Sciences, University of Birmingham, Edgbaston, B15 2TT,
Birmingham, UK
e-mail: dmf144@adf.bham.ac.uk

O. den Braver

BioMechanical Engineering, Delft University of Technology, Mekelweg 2, 2628 CD Delft,
The Netherlands

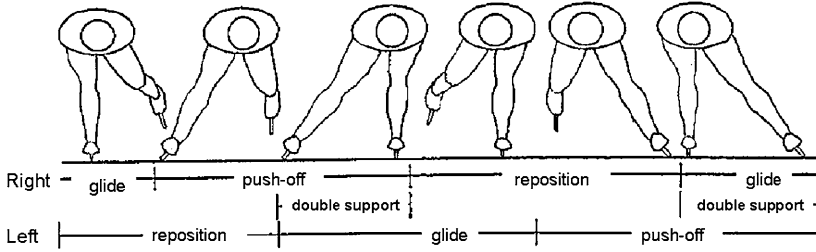


Fig. 1 Phases of a stroke: push-off phase, glide phase and reposition phase [1]

of motion. In speed skating humans generate forces by pushing in sideward direction. When we take a closer look at speed skating the straights we observe that a skating stroke can be divided in three phases: the glide, push-off and reposition phase, see Fig. 1. In the push-off phase the skate moves sideways with respect to the center of mass (COM) of the body till near full leg extension. In the reposition phase the leg is retracted in the direction of the center of mass of the body. During the glide phase the body is supported over one leg that remains at nearly constant height (ankle to hip distance). Double support, where both skates are on the ice, only exists in the first part of the glide phase of one leg and in the second part of push-off phase of the other leg. This coordination pattern with sideward push-off results in a sinus-wave like trajectory of the upper body on the ice [4].

From these observations a number of questions arise. Of the many possible coordination patterns, that is position and orientation of the skates with respect to the upper body, why do skaters use this particular one? What is the optimal coordination pattern for an individual speed skater to reach their optimal performance? How do speed skaters create forward power on ice? Why are speed skaters steering back to their body at the end of the push-off? What is the effect of anthropometric differences on the coordination pattern of a speed skater (like the difference between a tall Dutch skater and a small Japanese skater)? All these questions are highly dependent on the coordination pattern of the speed skater and could well be addressed by simulation and optimization of a biomechanical model of speed skating. But before getting to this optimization approach one needs a model that reasonable matches observed behavior.

Currently, there exist three speed skating models [1, 6, 10]. The first models of speed skating were initiated by Gerrit Jan van Ingen Schenau [12] and further developed by researchers at the VU University Amsterdam [6]. By using power balances of the human and the environment useful information about the posture, athlete physiology and environmental parameters on the performance is obtained. Disadvantages of these models are that the validation is difficult and it is impossible to investigate differences in coordination pattern.

A more recent model was developed by Otten [10], in which forward and inverse dynamics are combined. The model is complex and includes up to 19 rigid bodies and 160 muscles. The model is able to simulate skating and can give insight in the forces/moments in the joints. Limitations of the model are that the kinematics in

the model are manually tuned and that the model is not driven and validated with measurements of speed skaters. Unfortunately, no information about this model is available in the open literature, which makes it hard to review.

The most recent speed skater model is developed by Allinger and van den Bogert [1]. they developed a simple, one point mass, inverse dynamics model of a speed skater which is driven by individual strokes. The main limitations of the model are that the model is driven by a presumed leg function in time and that the model is not validated with force measurements. Furthermore, the effect of the assumptions on the model (e.g. constant height) are not investigated. On the other hand the model is possibly accurate and very useful for optimization the coordination pattern of speed skating.

Although three biomechanical models exist, none of these models is shown to accurately predict observed forces and motions. Which is partly due to the lack of experimental kinematic data and force data on stroke level.

In this chapter, we present a 2-dimensional inverse dynamics model on the straights which has minimal complexity. The model is based on three lumped masses and is validated with observed in-plane (horizontal) kinematics and forces at the skates. In the future, this model can be used to provide individual advice to elite speed skaters about their coordination pattern to reach their optimal performance.

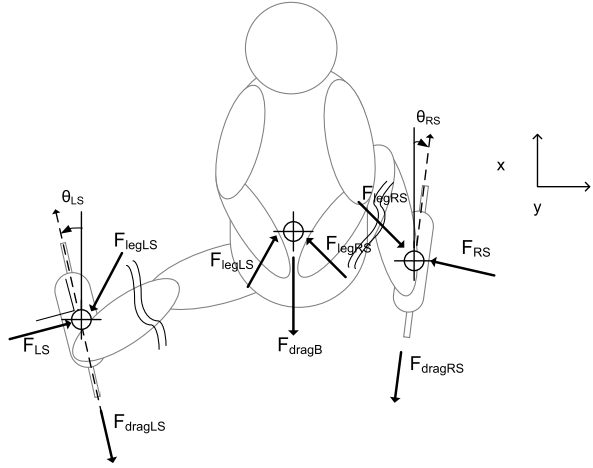
2 Methods

We measured in time the 2-dimensional in-plane (horizontal) positions (x, y) of the two skates and the upper body, the normal forces and lateral forces at the two skates and lean angle of the skates. We developed a 2-dimensional inverse dynamic model of a skater. The model is driven by the measured leg extensions, that is relative motions of the skates with respect to the upper body and absolute orientation of the skates with respect to the ice. The upper body motions together with the forces exerted on the ice by the skates are calculated from the model.

A schematic of our 2-dimensional model is shown in Fig. 2. The model consists of three point masses: lumped masses at the body and the two skates. The total mass of the system is distributed over the three bodies by a constant mass distribution coefficient. The motions of the arms are neglected. We do not consider the vertical motion of the upper body, since experiments show that the upper body is at nearly constant height [3]. Air friction and ice friction are taken into account. Idealized contact of the skate on the ice is modeled by a holonomic constraint in the vertical direction and a non-holonomic constraint in the lateral direction.

Values for the mass distribution and air friction are found experimentally. The best agreement between the measurements and model can be achieved if we use accurate values for these parameters. Therefore we constructed an objective function J_{\min} and minimized the error between the measurements and model. Details on the objective function can be found in Appendix 8.3.

Fig. 2 Free body diagrams of the three point mass model (horizontal plane, top view). The masses are located at the COM of the body and at the COM of the skates. F_{lS} and F_{rS} are perpendicular with the skate blades, θ_{lS} and θ_{rS} are the steer angles of the skates with respect to the x -axis. The x - and y -axes are the inertial reference frame fixed to the ice rink



3 Model Analysis

In the model analysis for speed skating, three stages can be distinguished. First, the unconstrained equations of motion of the speed skater of a single stroke are derived. Secondly, the constraints are formulated and incorporated into the unconstrained equations of motion. Finally all equations are derived in terms of generalized coordinates and solved by numerical integration of these constrained equations of motion.

3.1 Equations of Motion

The equations of motion for each separate body (upper body, right skate and left skate) can be derived in x and y direction. Friction forces (air and ice friction) as well as the constraint forces are acting on the bodies. All constraints acting on the bodies will be explained in the next paragraph. The unconstrained equations of motions for all bodies are,

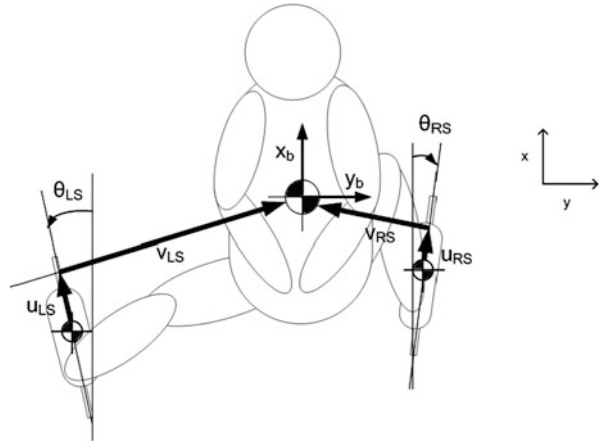
$$\begin{aligned} m\ddot{x}_i &= -F_{frictionX_i} + F_{constraintsX_i} \\ m\ddot{y}_i &= -F_{frictionY_i} + F_{constraintsY_i} \end{aligned} \quad i = B, LS, RS \quad (1)$$

where $F_{frictionX_i}$ is the component of the friction force in x direction and $F_{frictionY_i}$ the component of the friction force in y direction. $F_{constraintsX}$ are the constraint forces in x direction and $F_{constraintsY}$ the constraint forces in y direction.

3.2 Constraints

The first set of constraints are the leg extension constraints, they connect the skates to the upper body. The positions of the skates are prescribed by the position of the

Fig. 3 Definition of generalized coordinates



upper body and the leg extension coordinates. The second set of constraints are at the skates. A holonomic constraint is applied in the vertical direction which establish that the skate is on the ice and a non-holonomic constraint in the lateral direction of the skate to express that there is no lateral slip of the skate on the ice.

3.3 Generalized Coordinates

The generalized coordinates of the skater model are chosen such that we can express the coordination of the motion of the skater in terms of the leg extensions and the skate orientations (steer angles). Therefore the configuration of the skater is expressed by the motion of the upper body and the leg extensions (relative motions of the skates with respect to the upper body, see Fig. 3) and can be described by the generalized coordinates,

$$\mathbf{q} = (x_b, y_b, u_{LS}, v_{LS}, \theta_{LS}, u_{RS}, v_{RS}, \theta_{RS})^T, \quad (2)$$

in which θ_{LS} and θ_{RS} are the steer angles of the skates with respect to the global x -axis. These steer angles, which are prescribed coordinates, are needed to apply the non-holonomic skate constraints. The equations of motion will be written in terms of the generalized coordinates. Detailed information on the transformation of the equations of motions in terms of the generalized coordinates can be found in Appendices 8.1, 8.7, and 8.8.

3.3.1 Leg Extension Constraints

The position of the right and left skate can be expressed as function of the generalized coordinates and will be incorporated into the equations of motion means by holonomic constraints. The left skate leg extension constraints are,

$$c_1 = x_{LS} - x_B + \cos(\theta_{LS})u_{LS} + \sin(\theta_{LS})v_{LS} = 0, \quad (3)$$

$$c_2 = y_{LS} - y_B - \sin(\theta_{LS})u_{LS} + \cos(\theta_{LS})v_{LS} = 0, \quad (4)$$

and the right skate leg extension constraints are,

$$c_3 = x_{RS} - x_B + \cos(\theta_{RS})u_{RS} + \sin(\theta_{RS})v_{RS} = 0, \quad (5)$$

$$c_4 = -y_{RS} + y_B - \sin(\theta_{RS})u_{RS} + \cos(\theta_{RS})v_{RS} = 0. \quad (6)$$

3.3.2 Skate Constraints

When the skate is on the ice we assume no lateral slip between the ice and skate, that is the lateral velocity of the skate is zero. This can be expressed by a non-holonomic constraint which are for the left and right skate respectively,

$$c_5 = -\sin(\theta_{LS})\dot{x}_{LS} - \cos(\theta_{LS})\dot{y}_{LS} = 0, \quad (7)$$

$$c_6 = -\sin(\theta_{RS})\dot{x}_{RS} + \cos(\theta_{RS})\dot{y}_{RS} = 0. \quad (8)$$

Since we do not consider vertical motions no constraints in the vertical direction are needed. Contact or no contact is described by on/off switching of the corresponding non-holonomic constraint.

3.4 Mass Distribution

The number of bodies in the model is based on an investigation of the shift in position of the center of mass on a complete anthropometric model of a speed skater during the gliding and the push-off phase of a stroke. A minimum of three bodies was shown to be necessary for describing the shift of the center of mass [8].

The total mass m of the skater is now distributed over the three point masses (body, left skate, right skate) by using a mass distribution coefficient α (Fig. 4). The distribution of the masses are given by $m_B = (1 - \alpha)m$, $m_{LS} = (\alpha/2)m$, and $m_{RS} = (\alpha/2)m$.

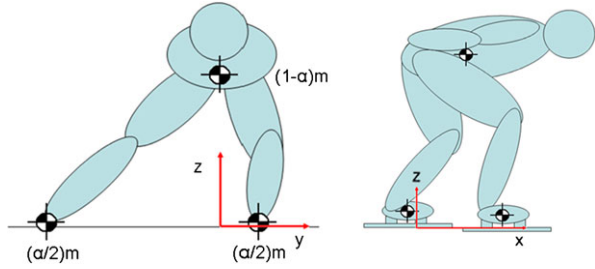
3.5 Friction Forces

The total friction forces can be roughly divided in 80 % air friction and 20 % ice friction [5]. The ice friction in the model, following de Koning [7], is described by Coulomb's friction law,

$$F_{\text{ice}} = \mu F_N \quad (9)$$

where μ is the friction coefficient and F_N the normal force of the skate on the ice. Here we assume that the height of the skater is constant and that there is no double

Fig. 4 Positions of the COM of the bodies during the push-off together with the mass distribution



stance phase. Therefore, the ice friction can be written as $F_{\text{ice}} = \mu mg$, in which m the total mass of the skater and g the earth gravity. The air friction can be described by,

$$F_{\text{air}} = \frac{1}{2} \rho C_d A v^2 = k_1 v^2 \quad (10)$$

where ρ represents the air density, C_d the drag coefficient, A the frontal projected area of the skater, and v the velocity of the air with respect to the skater. The air drag forces at each individual mass are calculated by multiplying the mass distribution coefficient of that mass by the total air drag. The drag coefficient k_1 can only be estimated experimentally. With an experimental method (see Appendix 8.5) both the drag coefficients μ and k_1 for every individual subject are estimated.

3.6 Model Summary

The equations of motion together with the constraint equations are completely defined by the state of skater. Combining the equations of motion for the individual masses (1) and including of the constraint forces and the constraints (3)–(6) on the acceleration level results in the constraint equations of motion for the system, $\mathbf{A}\mathbf{u} = \mathbf{b}$, with

$$\mathbf{A} = \begin{bmatrix} m(1-\alpha) & 0 & 0 & 0 & 0 & 0 & -1 & 0 & -1 & 0 \\ 0 & m(1-\alpha) & 0 & 0 & 0 & 0 & 0 & -1 & 0 & 1 \\ 0 & 0 & \frac{\alpha}{2}m & 0 & 0 & 0 & 1 & 0 & 0 & 0 \\ 0 & 0 & 0 & \frac{\alpha}{2}m & 0 & 0 & 0 & 1 & 0 & 0 \\ 0 & 0 & 0 & 0 & \frac{\alpha}{2}m & 0 & 0 & 0 & 1 & 0 \\ 0 & 0 & 0 & 0 & 0 & \frac{\alpha}{2}m & 0 & 0 & 0 & -1 \\ \hline -1 & 0 & 1 & 0 & 0 & 0 & 0 & 0 & 0 & 0 \\ 0 & -1 & 0 & 1 & 0 & 0 & 0 & 0 & 0 & 0 \\ -1 & 0 & 0 & 0 & 1 & 0 & 0 & 0 & 0 & 0 \\ 0 & 1 & 0 & 0 & 0 & -1 & 0 & 0 & 0 & 0 \end{bmatrix} \quad (11)$$

$$\mathbf{u} = [\ddot{x}_B \quad \ddot{y}_B \quad \ddot{x}_{LS} \quad \ddot{y}_{LS} \quad \ddot{x}_{RS} \quad \ddot{y}_{RS} \quad \lambda_1 \quad \lambda_2 \quad \lambda_3 \quad \lambda_4]^T \quad (12)$$

$$\mathbf{b} = \begin{bmatrix} -F_{XfrictionB} & -F_{YfrictionB} & -F_{XfrictionLS} & -F_{YfrictionLS} & -F_{XfrictionRS} \\ -F_{YfrictionRS} & h_{c1} & h_{c2} & h_{c3} & h_{c4} \end{bmatrix}^T \quad (13)$$

where $h_{c1} \dots h_{c4}$ are the convective acceleration terms of the constraints (Appendix 8.8) and $\lambda_1 \dots \lambda_4$ are the constraint forces (Lagrange multipliers). Here λ_1 and λ_2 are the constraint forces in the left leg, and λ_3 and λ_4 the constraint forces in the right leg. The non-holonomic skate constraints are not yet included in this system, but will be in a later stage.

The model consists of 3 bodies with each 2 degrees of freedom, thus the unconstrained system has 6 degrees of freedom. However, there are 4 coordination constraints and 1 non-holonomic constraint of the skate on the ice (no double stance); therefore 1 degree of freedom remains. If there is a double stance phase then both skates are on the ice, the system is over-constrained and no degree freedom is left. Therefore for the model we will assume only single stance phases, and the model will alternatively switch between the right skate en left skate constraint. This assumption is validated by the experimental force data, where we see only a short period of double stance with load transfer.

We rewrite the equations of motion (11)–(13) (still without the non-holonomic skate constraints) in terms of the generalized coordinates (2), where the prescribed coordinates (leg extension coordinates $(u_{LS}, v_{LS}, \theta_{LS}, u_{RS}, v_{RS}, \theta_{RS})$) are pushed to the right-hand side (Appendix 8.1). Next, the constraint of the skate on the ice (left or right) is added to the equations. Finally the reduced constrained equations of motion are given by, for when the left skate is on the ice,

$$\begin{bmatrix} m & 0 & -s_{LS} \\ 0 & m & -c_{LS} \\ -s_{LS} & -c_{LS} & 0 \end{bmatrix} \begin{bmatrix} \ddot{x}_B \\ \ddot{y}_B \\ \lambda_5 \end{bmatrix} = \begin{bmatrix} \mathbf{T}_{\mathbf{q}}^T(\mathbf{f} - \mathbf{M}\mathbf{h}) \\ h_{c5} \end{bmatrix}, \quad (14)$$

and for when the right skate is on the ice,

$$\begin{bmatrix} m & 0 & -s_{RS} \\ 0 & m & c_{RS} \\ -s_{RS} & c_{RS} & 0 \end{bmatrix} \begin{bmatrix} \ddot{x}_B \\ \ddot{y}_B \\ \lambda_6 \end{bmatrix} = \begin{bmatrix} \mathbf{T}_{\mathbf{q}}^T(\mathbf{f} - \mathbf{M}\mathbf{h}) \\ h_{c6} \end{bmatrix}, \quad (15)$$

where λ_5 and λ_6 are the lateral constraint forces on the skate and h_{c5} and h_{c6} are the convective acceleration terms of the skate constraints, the latter are presented in Appendix 8.8. Clearly both systems have one degree of freedom left, one can think of it as being the forward motion.

3.7 Model Constants

Experimental data was obtained from four different riders. Listed in Table 1 are the values of the model parameters used in the simulations for these four riders. The total mass of the skater and gravity are a measured quantities. The other parameters are found by an optimization process as described in Appendix 8.3.

Table 1 Parameter values for the four riders

Variable	Description	Value
m	Mass skater	66, 80, 77, 84 [kg]
α	Mass distribution	0.604, 0.682, 0.607, 0.686 [-]
k_1	Drag coefficient	0.160, 0.153, 0.112, 0.299 [N/(m/s) ²]
g	Gravity	9.81 [m/s ²]

4 Model Analysis

4.1 Parametrization of the Coordination Body Functions

Input to the model are the measured motion coordinations, the leg extensions and the skate steer angles, and their velocities and accelerations. To determine these all measured positions have to be differentiated with respect to time. To get rid of model errors due to numerical differential and filtering errors (spikes), all positions are first parameterized by smooth functions. The required parametrization functions have to be twice differentiable. The combination of a linear and periodic functions satisfies this requirement. The used parametrization function is,

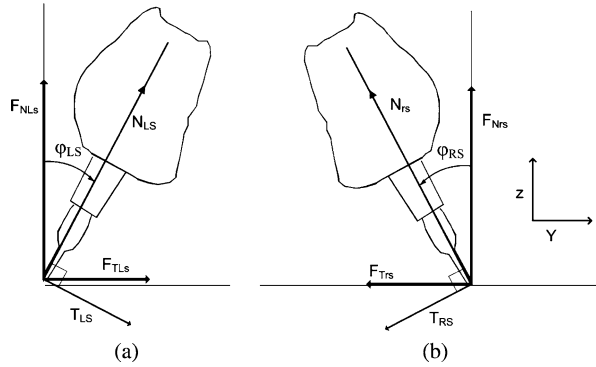
$$f = c_0 + c_1 t + \sum_{k=1}^5 a_k \sin\left(2k\pi \frac{t}{T}\right) + b_k \cos\left(2k\pi \frac{t}{T}\right). \quad (16)$$

The fit is not accurate at the beginning and end of the stroke, which results in a mismatch of the initial conditions on the velocities and accelerations. Therefore the coordinates are fit at a somewhat longer time period and then cut off afterwards. We tried also other parametrization functions, like polynomial and cubic splines. The differentials of polynomial functions became unstable with increasing order, while piecewise cubic splines have no filtering which results in high frequent components in the positions. The measured positions of the body, left and right skate in x and y direction of a single stroke are parameterized according to (16) and by differentiating the equations of the fitted function the velocities and acceleration are calculated.

4.2 Integration of the Differential Equations

The differential algebraic equations (14), (15) describing the motion of the system cannot be solved analytically. Therefore, the equations will be numerically integrated, using the classic Runge-Kutta 4th order method (RK4). The stepsize h is taken constant during the whole simulation, and chosen identical to the sample time of the measurements $T_s = 1/100$ [sec]. After each numerical integration step the constraints are fulfilled by a projection method (Appendix 8.2).

Fig. 5 Forces in local reference frame (N_{ls} , T_{ls} , N_{rs} , T_{rs}) and global reference frame (F_{Nls} , F_{Tls} , F_{Nrs} , F_{Trs}): (a) Left skate, (b) right skate



4.3 Data Collection

The data collection of the skater includes the 2-dimensional in-plane positions (x , y) of the two skates and the upper body, the normal and lateral forces at the two skates and lean angle of the skates. The global positions are measured by a radio frequency based so-called local position measurement system (LPM) from Inmotio.¹ This system is installed at the Thialf speed skate rink in Heerenveen, The Netherlands. The LPM system has been used for analysis of soccer matches, and can handle up to 22 active transponders at 1000/22 Hz. The transponders are approximately placed at the positions of the point masses.

We have developed two instrumented clap skates to measure the normal and lateral forces (N_i , L_i) at the blades of the skates, see Fig. 5. To be able to compare these with the model output, which are the global lateral forces F_{Tls} and F_{Trs} , the lean angles of the skates, ϕ_i , has to be measured too. These angles are measured using an inertial measurement unit from Xsens,² where only the lean angle is used.

For data acquisition a DAQ unit of National instruments³ is used. All the force and orientation data is collected from the DAQ via a USB connection on a mini laptop which is carried by the skater in a backpack. The different measurement systems are synchronized by means of images from a high speed camera. See Appendix 8.4 for detailed description of the synchronization method.

Data sets of four trained speed skaters are used to validate the model. The data collection is performed with a standard measurement protocol which includes: skating two laps at an estimated 80 % of maximal performance level. The tests are repeated at least three times.

¹<http://www.inmotio.nl>, Hettenheuvelweg 8, 1101 BN Amsterdam Zuidoost, The Netherlands.

²<http://www.xsens.com>.

³<http://www.ni.com>.

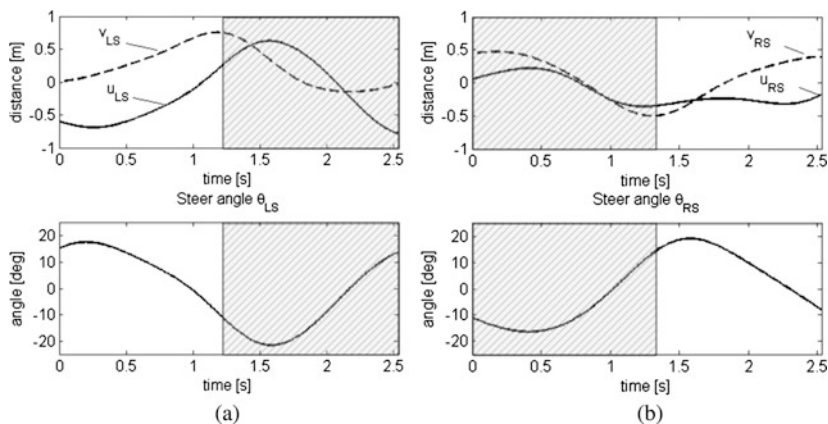


Fig. 6 Measured and parameterized leg extension coordinates u_i , v_i and θ_i as a function of time for a sequencing left and right stroke for rider 1 from Table 1. *Gray filled area* means that the skate is not active. (a) Left skate, (b) right skate

4.4 Fitting the Model to the Observed Data

The model is validated by showing how closely it can simulate the observed forces and motions. Quantification of the model errors are analyzed similar to that of McLean [9]. The measured data has different scales and units and therefore we constructed a measurement of error, J_{\min} , between the model and the measured data which includes the error of the upper body position, velocities and local normal forces (N_{lS} and N_{rS}). The measurement of error is dimensionless, reasonably scaled and independent of the number of time samples. See Appendix 8.3 for a detailed description of the measurement error function J_{\min} .

5 Results

Plots of the measured and simulated forces and motions (output of model) as a function of time for a sequencing left and right stroke are shown in Fig. 7 (the parameters are according to the first rider from Table 1). The corresponding measured and parameterized leg extensions (input of model) of the left and right leg are shown respectively in Fig. 6(a) and Fig. 6(b). At the beginning of the left stroke ($t = 0$) the skate is placed in front of the upper body, resulting in a negative u_{lS} . During the stroke the skate is moving sideways and backwards, u_{lS} and v_{lS} increase. At the end of the stroke the skate is retracting to the upper body, u_{lS} and v_{lS} decrease. At the beginning of the right stroke ($t = 1.25$), the skate is again moving sideways, v_{rS} increase. However the motion pattern of the u_{rS} is somewhat different in comparison with u_{lS} . The u_{rS} remains approximately constant during the stroke, which eventually will result in a different output motion of the upper body in y direction.

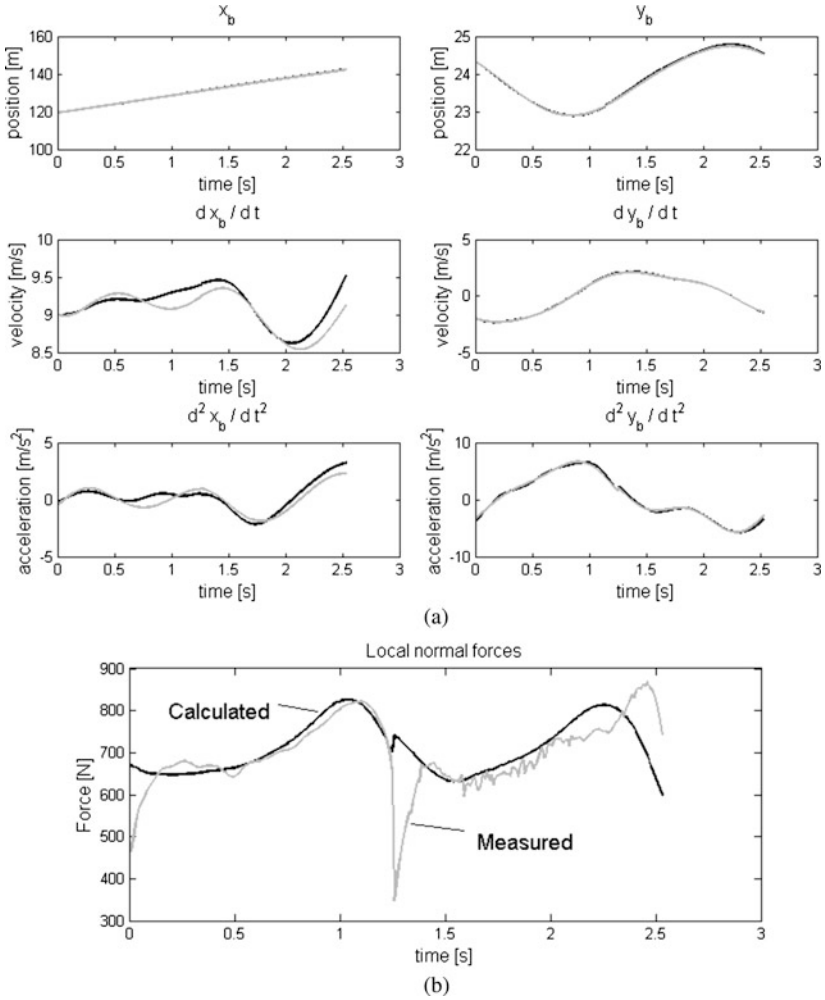


Fig. 7 Simulated (*black lines*) and measured (*gray lines*) upper body positions, velocities, accelerations and local normal forces on the skates (N_i), as a function of time for a sequencing left and right stroke, for rider 1 from Table 1 ($mg = 647$ N)

The skater has an average forward speed of ≈ 32 km/h. The upper body describes a sine-wave like trajectory with respect to the ice during speed skating the straights (Fig. 7(a), y_b), which has also been observed by de Boer [4]. The velocity pattern sideways, \dot{y}_b , are alike for left and right stroke. However, the forward acceleration/deceleration pattern differ per stroke. This was observed for every rider.

The local normal forces N_{LS} and N_{RS} of the active skate are shown in Fig. 7(b), where the height of the body is assumed constant. At the large force drop in the measured force data a switch is made in the model from the left skate to the right

Table 2 Net error J_{\min} per subject (average of all left straight strokes of all tests) divided by the number of optimization parameters

Skater	J_{\min}
1	0.0013
2	0.0015
3	0.0022
4	0.0013

skate. Note that the sum of the measured left and right force corresponds well to the calculated value. At the beginning of the stroke the normal force is rising above the body weight of the skater. Then a small force drop appears and at the end of stroke the normal forces rises again well above the body weight. The maximal normal force during push-off is approximately 150 % of the body weight.

Agreement exists between the measured and simulated positions and velocities. The largest error is in the force data, which mainly appears at the beginning and end of the stroke.

For all skaters the net error J_{\min} (24) of all straight left strokes is calculated. This net error is divided by the number of optimization parameters being the upper body positions, upper body velocities and the local normal forces and presented in Table 2.

Averages of the magnitudes of the residuals are calculated similar to that of Cabrera [2] by $R_j = \sum_{i=1}^N |\tilde{y}_{ij} - y_{ij}|/N$. In which N the number of collected data points, y_i the measured value of the variable and \tilde{y}_i the simulated value of the variable from the model. For all variables j the R_j is shown in Table 3. The residuals of the upper body are less than 0.10 m for the forward position, 0.031 m sideways, 0.20 m/s in the forward velocity, 0.06 m/s sideways, and 53 N for the local normal forces in the skate.

Table 3 Table of the residuals between measured and simulated values of the variables. Body position in x direction [m], body position in y direction [m], body velocity in x direction [m/s], body velocity in y direction [m/s], body acceleration in x direction [m/s^2], body acceleration in y direction [m/s^2], local normal forces [N]

Skater	R_{xb}	R_{yb}	$R_{\dot{x}b}$	$R_{\dot{y}b}$	$R_{\ddot{x}b}$	$R_{\ddot{y}b}$	R_{Nl}
1	0.0795	0.0165	0.1769	0.0464	0.5880	0.3836	22.01
2	0.0817	0.0245	0.1659	0.0491	0.5952	0.3379	34.30
3	0.1048	0.0314	0.2071	0.0626	1.0276	0.3244	53.91
4	0.0782	0.0186	0.1737	0.0401	0.8315	0.2380	26.45

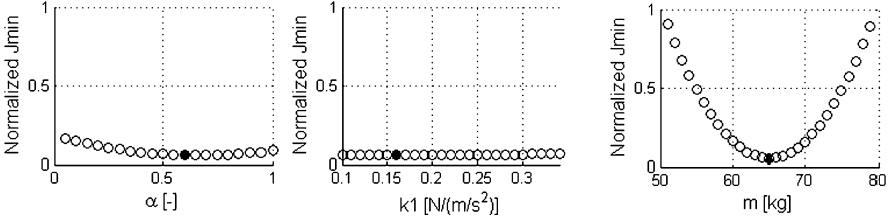


Fig. 8 Plots of J_{\min} versus a single parameter value, mass distribution α , air friction coefficient k_1 and total mass of the skater m , as the parameter is varied about the nominal value for rider 1 from Table 1. The *filled circles* correspond to the value of J_{\min} at the nominal parameter value

6 Discussion

6.1 Model Error

All position residuals are within the accuracy of the position measurement system (≈ 0.15 m). The accuracy of the LPM can be increased if two transponders, instead of one transponder are positioned at the skates and the upper body. The forward velocities \dot{x}_B are less accurate than the sideward velocities \dot{y}_B , which is reasonable due to the fact that the forces are mainly in sideward direction instead of forward. Orientation errors have therefore more influence on the \dot{x}_B than on the \dot{y}_B .

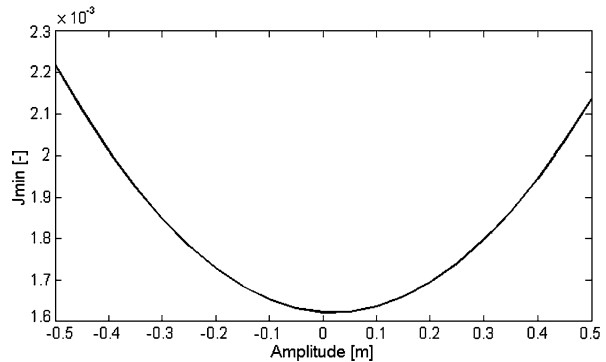
No total agreement exists between the measured forces and the forces calculated in the model, generally at the beginning and at the end of the stroke. There is no normal force drop in the calculated data which is a result of the simplification that there is no double stance phase, but the sum of the measured left and right force do correspond well with the calculated one. Conversion from global to local forces resulted in a force error, caused by the accuracy of the lean angle sensors. The accuracy of these sensors are < 2 deg root mean square, resulting in a local normal force error between $\approx 20/-20$ N. Besides conversion errors, crosstalk exists of $\approx 3\%$ of the lateral forces to the normal forces (max. $-9/9$ N). The maximal error due to inaccuracy of the measurement equipment is then approximately 29 N.

The net error J_{\min} of all measurements are in the same magnitude, which shows that the model is valid for all subjects.

6.2 How Does the Fit Depend on Mechanical Constants

The sensitivity of the mechanical constants is obtained by minimizing the net error J_{\min} (24). This net error is calculated by letting the upper body motions variable while fixing all other parameters to their optimal fit value, except for the wanted minimization parameter (mass distribution α , air friction coefficient k_1 or mass of the skater m). In Fig. 8 the normalized net error J_{\min} are plotted as function of the minimization parameters. The minimal values in the figures correspond to the values of the parameters at the optimal fit.

Fig. 9 Plot of error J_{\min} versus the amplitude of the sine wave corrupting the velocity data of the upper body of the skater



The mass is the most sensitive mechanical parameter, however this parameter is measured accurately and therefore of no concern here. The value of the mass distribution α as well as the friction coefficient k_1 are more uncertain. The figure shows clearly that the fit depends little on these mechanical constant.

6.3 Fitting False Data

If the fits which are obtained are a result of good curve fitting, then it should be able to obtain good fits to false data. To test the model a pure sine function, $A \cos(2\pi t/T)$, with amplitude A , and stroke time T , is added to the measured velocity data of the upper body in either directions. In Fig. 9 the minimal error function versus the amplitude of the sinus wave is plotted. The total error between the model and the measured variables is minimal if the amplitude of the added function is zero. The model shows the best fit if there is not added corrupted data to the velocity data of the upper body. These results shows that the fits are not a result of good curve fitting, but rather the result of a good model.

6.4 Kinematic Complexity

The double stance phase was not included in the model. However, the sum of the measured left and right force during the short double stance phase do correspond well with the calculated forces (Fig. 7(b)), which demonstrates that there is little need for modeling this double stance phase.

Another major simplification of the model is that it was assumed that the center of mass remains at a constant height during skating, which was based on de Boer [3]. However, in accelerometer data of the upper body it was found that at the end of the stroke the upper body accelerates about 1.5 times gravity, which really influences the forces in the model. Therefore it seems beneficial to include the vertical motion of the body in the model.

7 Conclusions

We have constructed a simple 2-dimensional model of speed skating that does a reasonable job of imitating the forces and kinematics as observed in actual speed skating. The model reproduces these forces and motions reasonably well, even if we do not fit for that. The model is limited in accuracy due to the limited accuracy of the LPM position measurement system. Adding the (small) vertical motion of the upper body can increase the accuracy of the model.

The model seems promising for individual training advice. Coordination patterns of individual skaters can be optimized by using the model if psychological constraints of individual skater are added to the model. In Appendix 8.6 a detailed description of the needed constraints on the model is given. The model can also be used to give insight in the biomechanics of speed skating, like why speed skaters steer back to their body at the end of the stroke. Finally the effect of anthropometric differences between speed skaters can be determined.

Appendix

This appendix contains details on the modeling and the experimental validation and comments and remarks for future use of the model for optimization of speed skater performance.

8.1 Kinematic Transformation

This section describes the transformation of the equations of motion in terms of the generalized coordinates.

We start with the differential algebraic (constraint) equations of motion (DAEs), without the non-holonomic skate constraint, from (11), which can be written as,

$$\begin{bmatrix} \mathbf{M} & \mathbf{C}^T \\ \mathbf{C} & \emptyset \end{bmatrix} \begin{bmatrix} \ddot{\mathbf{x}} \\ \boldsymbol{\lambda} \end{bmatrix} = \begin{bmatrix} \mathbf{f} \\ \mathbf{h}_c \end{bmatrix}, \quad (17)$$

with the COM accelerations $\ddot{\mathbf{x}}$, the diagonal mass matrix \mathbf{M} , the applied forces \mathbf{f} at the COM, the Jacobian $\mathbf{C} = \partial \mathbf{c} / \partial \mathbf{x}$ of the constraint equations $\mathbf{c}(\mathbf{x}) = 0$, the convective terms $\mathbf{h}_c = (\partial(\mathbf{C}\dot{\mathbf{x}}) / \partial \mathbf{x})\dot{\mathbf{x}}$, and the Lagrange multipliers $\boldsymbol{\lambda}$, with respect to the constraints \mathbf{c} . The constrained equations of motion are,

$$\mathbf{M}\ddot{\mathbf{x}} = \mathbf{f} - \mathbf{C}^T \boldsymbol{\lambda}. \quad (18)$$

Next, we like to rewrite the equations in terms of the generalized coordinates \mathbf{q} . Therefore we introduce the coordinates of the COM \mathbf{x} expressed in terms of the generalized coordinates \mathbf{q} ,

$$\mathbf{x} = \mathbf{T}(\mathbf{q}). \quad (19)$$

Differentiate this twice with respect to time,

$$\dot{\mathbf{x}} = \mathbf{T}_{,q}\dot{\mathbf{q}} \quad \text{and} \quad \ddot{\mathbf{x}} = \mathbf{T}_{,q}\ddot{\mathbf{q}} + \mathbf{h}. \quad (20)$$

The subscript comma followed by one or more variables denotes the partial derivatives with respect to these variables, and with the convective terms $\mathbf{h} = (\mathbf{T}_{,q}\dot{\mathbf{q}})_{,q}\dot{\mathbf{q}}$. Substitution of these accelerations in (18) and pre-multiplying with the transposed Jacobian $\mathbf{T}_{,q}^T$ gives,

$$\mathbf{T}_{,q}^T \mathbf{M}(\mathbf{T}_{,q}\ddot{\mathbf{q}} + \mathbf{h}) = \mathbf{T}_{,q}^T (\mathbf{f} - \mathbf{C}^T \boldsymbol{\lambda}). \quad (21)$$

Since the generalized coordinates fulfill the constraints, $\mathbf{T}_{,q}^T \mathbf{C}^T$ is identical to zero, that is the constraint forces $\boldsymbol{\lambda}$ drop out of the equations. The result is the equations of motion expressed in terms of the generalized coordinates \mathbf{q} ,

$$\mathbf{T}_{,q} \mathbf{M} \mathbf{T}_{,q}^T \ddot{\mathbf{q}} = \mathbf{T}_{,q}^T (\mathbf{f} - \mathbf{M} \mathbf{h}). \quad (22)$$

Finally the skate constraint can be added to these equations of motion, which results in the constraint equations of motion (14) and (15).

8.2 State Projection

After numerical integration of the equations of motion for one time increment, the state variables in general do not fulfill the constraints. This can be solved by formulating a minimization problem such that the distance from the predicted solution $\tilde{\mathbf{q}}_{n+1}$ to the solution which is on the constraint surface \mathbf{q}_{n+1} is minimal: $\|\tilde{\mathbf{q}}_{n+1} - \mathbf{q}_{n+1}\|_2 = \min_{\mathbf{q}_{n+1}}$ and where all \mathbf{q}_{n+1} have to fulfill the constraints $\mathbf{c}(\mathbf{q}_{n+1}) = 0$. This non-linear constraint least-square problem is in general solved with a Gauss-Newton method after every numerical integration step. However, here we have to deal with non-holonomic constraints only, which are linear in the speeds $\mathbf{C}(\mathbf{q}_{n+1})\dot{\mathbf{q}}_{n+1} = 0$. The optimization problem then reduces to a linear constraint least-square problem which can be solved in one step.

8.3 Objective Function J_{\min}

The best agreement between simulation and measurements can be achieved if we use accurate values for the air friction coefficient and the mass distribution. This is solved by minimizing the error between the model and the measurements. The objective function is defined by equation:

$$E_j = \frac{1}{N} \sum_{i=1}^N (\tilde{y}_i - y_i)^2 \quad (23)$$

where N the number of collected data points, y_i the measured value of the variable and \tilde{y}_i the simulated value of the variable from the model. This is a constrained

multivariable minimization problem: $\min_x f(x)$ with the constraint: $lb \leq x \leq ub$ in which x are the air friction coefficient k_1 and mass distribution constant α . The upper and lower limit of α are defined as 0 and 1 while the limits of k_1 are defined as 0.1 and 0.3. With the optimization function *fmincon* of Matlab the optimal combination of α and k_1 are found. The optimization function uses an interior point algorithm and starts at the initial guess of the minimum x_0 . For each measured variable the optimal mechanical parameters can be fit.

Besides calculating the optimal values by minimizing one variable, the net error is calculated including the error of the upper body position, velocities and local normal forces (N_i). The net error is calculated with:

$$J_{\min} = \frac{\sum_{j=1}^M w_j \left(\frac{1}{N} \sum_{i=1}^N \frac{(\tilde{y}_{ij} - y_{ij})^2}{\bar{y}_j^2} \right)}{\sum_{j=1}^M w_j \bar{y}_j^2} \quad (24)$$

in which \tilde{y}_{ij} is the simulated value of a variable, y_{ij} the measured value of a variable, w_j is the weighting factor of a variable and \bar{y}_j is the characteristic value of the variable. The peak to peak values of the x and y upper body positions, average value of the body velocity in forward direction, peak to peak value of the velocity in sideward direction and the local measured normal peak force are used as the characteristic values of the parameters. Equal weights are used ($w_j = 1$) for all j in the error function.

8.4 Synchronization Method

The LPM position measurement system and the DAQ data acquisition unit are synchronized with video frames from a high speed (300 Hz) digital photo camera.⁴

8.4.1 Synchronization LPM and Video

The LPM is synchronized by using an extra static transponder, which was placed in line with the start line on the ice. During the synchronization test the line is filmed with the high speed camera (300 Hz). The moment of crossing the start line can be found in the LPM data and video.

8.4.2 DAQ and Video

In order to synchronize the DAQ and video frames a reset button with LED, which lights up when pressed, is used. The reset button is connected with the DAQ. At the start and the end of the measurement the subject has to push the reset button in view of the high speed camera, such that the video frames at which the LED reset button when pushed lights up can be easily determined.

⁴Casio Exilim EX-F1.

8.5 Friction Estimation

In order to estimate the friction coefficients, the subjects got the following instruction: after skating two laps immediately stop skating and glide along the line of the lanes in the same skating posture as you were skating before for 100 m.

In order to determine the coefficients of friction from the glide exercise, it is assumed that the friction coefficients are constant during the glide.

From this estimation the conclusion is drawn that the speed should decrease linearly. A first order polynomial is fitted through the velocity profile of the LPM data of the COM of the skater during gliding.

$$\dot{y}(t) = -at + b. \quad (25)$$

The gradient a of the line is the decelerations of the skater during gliding. The total friction force F_{friction} is the total mass m times the deceleration a of the skater during gliding; $F_{\text{friction}} = ma$. The air friction coefficient is assumed to behave like,

$$F_{\text{air}} = k_1 v^2 = \beta F_{\text{friction}}, \quad (26)$$

with the velocity v of the center of mass of the skater, k_1 the air drag factor and β the friction distribution factor which is assumed to be 0.8. The ice friction is assumed to behave like Coulomb friction as in

$$F_{\text{ice}} = \mu mg = (1 - \beta)F_{\text{friction}}, \quad (27)$$

where μ is the Coulomb friction coefficient between the ice and the skate.

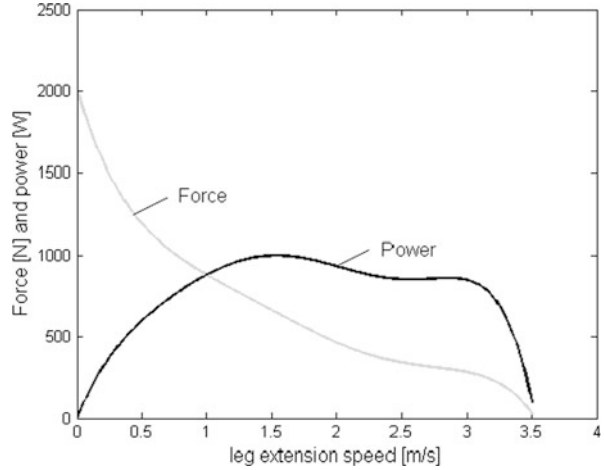
8.6 Optimization

For future application of the model where one wants to find coordination patterns which result in optimal performance, additional constraints are required. The model has to be constrained by the physiology of the skater during optimization of his coordination pattern. The physiology constraints of a skater are given by: the leg length, average power and maximal power of the speed skater.

8.6.1 Maximal Power Constraint

The maximal power during a single stroke must not exceed the maximal possible power from a leg extension motion of a skater. The maximal power constraint value could be based on either literature or experimentally determined. First, the maximal power can be determined from the push-off force and velocity of leg extension in the horizontal plane, since no work is done in the vertical plane. The maximal possible power of single leg extension as a function of the leg extension velocity can be based on force-velocity data extracted from leg press results of Vandervoort et al. [11]. The

Fig. 10 Force velocity relation [1]



power is estimated by multiplying the force with the extension velocity of the leg [1] (Fig. 10).

Secondly, the maximal power of a single leg extension could be experimentally determined per subject. In power models the maximal and average power of an athlete is measured with an ergometer test [6]. The measured ergometer power is then multiplied by an experimentally determined constant to determine the power during skating. However, the uncertainty on the constant is large so there is room for a better method to determine subject individual skating power.

8.6.2 Average Power Constraint

The average power of a stroke must not exceed the available aerobic power of a leg extension motion. The average power of a stroke can be calculated by:

$$P_{\text{avg}} = \frac{1}{t_{\text{stroke}}} \int_0^{t_{\text{stroke}}} P dt \quad (28)$$

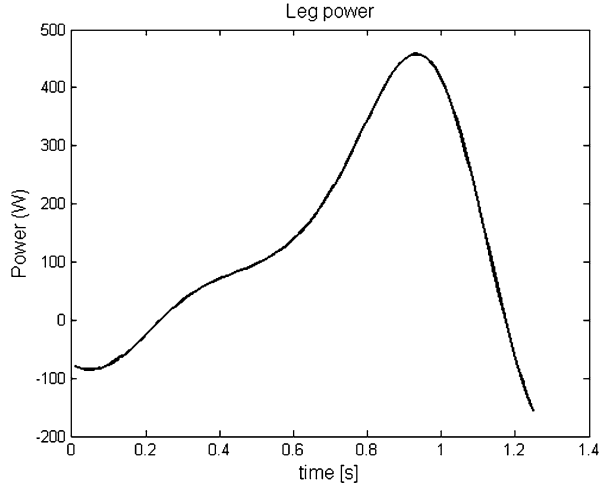
in which t_{stroke} is the stroke time and P is the available aerobic power for skating. For this equation it is assumed that the skater is running at steady state speed, which results in zero anaerobic power.

The average power exerted during skating can be either measured with oxygen measurements during the speed skating measurements or calculated by Eq. (28).

8.6.3 Leg Power Calculation

For optimization the power exerted by the skater of stroke has to fulfill the constraints. The power of a stroke can be determined from the push-off force of the

Fig. 11 Leg power in horizontal plane



skate on the ice and the leg extension in the horizontal plane, since no work is done in the vertical plane (Eq. (29)).

$$P_{leg} = F_{Tls} \dot{v}_{LS}. \quad (29)$$

An example of the leg power during a stroke can be seen in Fig. 11. At the beginning of the stroke the leg power becomes negative, which is caused by the negative direction of the lean angle. During the stroke the leg power increases to approximately 500 W. At the end of the stroke the extension speed decreases and the leg power becomes smaller.

8.7 Generalized Coordinates

The positions of the bodies (B , LS , RS) written in the generalized coordinates:

$$\begin{bmatrix} x_B \\ y_B \\ x_{LS} \\ y_{LS} \\ x_{RS} \\ y_{RS} \end{bmatrix} = \begin{bmatrix} x_B \\ y_B \\ x_B - \cos(\theta_{LS})u_{LS} - \sin(\theta_{LS})v_{LS} \\ y_B + \sin(\theta_{LS})u_{LS} - \cos(\theta_{LS})v_{LS} \\ x_B - \cos(\theta_{RS})u_{RS} - \sin(\theta_{RS})v_{RS} \\ y_B - \sin(\theta_{RS})u_{RS} + \cos(\theta_{RS})v_{RS} \end{bmatrix} \quad (30)$$

in which θ_i are the steer angles. These planar angular rotations can be calculated, since the velocity data of the skate in plane (x, y) are obtained. The skate steer angles are calculated by:

$$\begin{bmatrix} \theta_{LS} \\ \theta_{RS} \end{bmatrix} = \begin{bmatrix} -\tan^{-1}\left(\frac{\dot{y}_{LS}}{\dot{x}_{LS}}\right) \\ \tan^{-1}\left(\frac{\dot{y}_{RS}}{\dot{x}_{RS}}\right) \end{bmatrix}. \quad (31)$$

8.8 Convective Acceleration Terms

The convective acceleration terms of the leg extension constraints are:

$$\begin{aligned}
 h_{c1} = & \ddot{\theta}_{LS}(v_{LS} \cos(\theta_{LS}) - u_{LS} \sin(\theta_{LS})) + \ddot{u}_{LS} \cos(\theta_{LS}) + \ddot{v}_{LS} \sin(\theta_{LS}) \\
 & - \dot{\theta}_{LS}(\dot{\theta}_{LS}(u_{LS} \cos(\theta_{LS}) + v_{LS} \sin(\theta_{LS})) - \dot{v}_{LS} \cos(\theta_{LS}) + \dot{u}_{LS} \sin(\theta_{LS})) \\
 & + \dot{\theta}_{LS}\dot{v}_{LS} \cos(\theta_{LS}) - \dot{\theta}_{LS}\dot{u}_{LS} \sin(\theta_{LS})
 \end{aligned} \quad (32)$$

$$\begin{aligned}
 h_{c2} = & \ddot{v}_{LS} \cos(\theta_{LS}) - \ddot{\theta}_{LS}(u_{LS} \cos(\theta_{LS}) + v_{LS} \sin(\theta_{LS})) - \ddot{u}_{LS} \sin(\theta_{LS}) \\
 & - \dot{\theta}_{LS}(\dot{\theta}_{LS}(v_{LS} \cos(\theta_{LS}) - u_{LS} \sin(\theta_{LS})) + \dot{u}_{LS} \cos(\theta_{LS}) + \dot{v}_{LS} \sin(\theta_{LS})) \\
 & - \dot{\theta}_{LS}\dot{u}_{LS} \cos(\theta_{LS}) - \dot{\theta}_{LS}\dot{v}_{LS} \sin(\theta_{LS})
 \end{aligned} \quad (33)$$

$$\begin{aligned}
 h_{c3} = & \ddot{u}_{RS} \cos(\theta_{RS}) - \ddot{\theta}_{RS}(-v_{RS} \cos(\theta_{RS}) + u_{RS} \sin(\theta_{RS})) + \ddot{v}_{RS} \sin(\theta_{RS}) \\
 & - \dot{\theta}_{RS}(\dot{\theta}_{RS}(u_{RS} \cos(\theta_{RS}) + v_{RS} \sin(\theta_{RS})) - \dot{v}_{RS} \cos(\theta_{RS}) + \dot{u}_{RS} \sin(\theta_{RS})) \\
 & - \dot{\theta}_{RS}\dot{v}_{RS} \cos(\theta_{RS}) - \dot{\theta}_{RS}\dot{u}_{RS} \sin(\theta_{RS})
 \end{aligned} \quad (34)$$

$$\begin{aligned}
 h_{c4} = & \dot{\theta}_{RS}(\dot{\theta}_{RS}(-v_{RS} \cos(\theta_{RS}) + u_{RS} \sin(\theta_{RS})) - \dot{u}_{RS} \cos(\theta_{RS}) + \dot{v}_{RS} \sin(\theta_{RS})) \\
 & + \ddot{v}_{RS} \cos(\theta_{RS}) - \ddot{u}_{RS} \sin(\theta_{RS}) - \ddot{\theta}_{RS}(u_{RS} \cos(\theta_{RS}) + v_{RS} \sin(\theta_{RS})) \\
 & - \dot{\theta}_{RS}\dot{u}_{RS} \cos(\theta_{RS}) - \dot{\theta}_{RS}\dot{v}_{RS} \sin(\theta_{RS}).
 \end{aligned} \quad (35)$$

The convective acceleration terms of the skate constraints are:

$$\begin{aligned}
 h_{c5} = & \dot{\theta}_{LS}\dot{u}_{LS} - \ddot{v}_{LS} + \ddot{\theta}_{LS}u_{LS} + \dot{\theta}_{LS}\dot{x}_B \cos(\theta_{LS}) - \dot{\theta}_{LS}\dot{y}_B \sin(\theta_{LS}) \\
 h_{c6} = & \dot{\theta}_{RS}\dot{u}_{RS} - \ddot{v}_{RS} + \ddot{\theta}_{RS}u_{RS} + \dot{\theta}_{RS}\dot{x}_B \cos(\theta_{RS}) + \dot{\theta}_{RS}\dot{y}_B \sin(\theta_{RS}).
 \end{aligned} \quad (36)$$

References

1. Allinger, T.L., van den Bogert, A.J.: Skating technique for the straights, based on the optimization of a simulation model. *Med. Sci. Sports Exerc.* **29**(2), 279–286 (1997)
2. Cabrera, D., Ruina, A., Kleshnev, V.: A simple 1+ dimensional model of rowing mimics observed forces and motions. *Hum. Mov. Sci.* **25**, 192–220 (2006)
3. de Boer, R.W., Nislen, K.L.: The gliding and push-off technique of male and female Olympic speed skaters. *Int. J. Sport Biomech.* **5**, 119–134 (1989)
4. de Boer, R.W., Schermerhorn, P., Gademan, J., de Groot, G., van Ingen Schenau, G.J.: Characteristic stroke mechanics of elite and trained male speed skaters. *Int. J. Sport Biomech.* **2**, 175–185 (1986)
5. de Koning, J.J.: Biomechanical aspects of speed skating. PhD thesis, Free University of Amsterdam (1991). ISBN 90-9003956-2
6. de Koning, J.J., van Ingen Schenau, G.J.: Performance-determining factors in speed skating. In: Zatsiorsky, V. (ed.) *Biomechanics in Sport: Performance Enhancement and Injury Prevention*. Olympic Encyclopedia of Sports Medicine, vol. IX (2000). ISBN 978-0-632-05392-6
7. de Koning, J.J., de Groot, G., van Ingen Schenau, G.J.: Ice friction during speed skating. *J. Biomech.* **25**(6), 565–571 (1992)

8. Fintelman, D.M.: Literature study: biomechanical models for speed skating. MSc report, BioMechanical Engineering, Delft University of Technology (2010)
9. McLean, S.G., Su, A., van den Bogert, A.J.: Development and validation of a 3-D model to predict knee joint loading during dynamic movement. *J. Biomech. Eng.* **125**, 864–874 (2003)
10. Otten, E.: Inverse and forward dynamics: models of multi-body systems. *Philos. Trans. R. Soc. Lond.* **358**, 1493–1500 (2003)
11. Vandervoort, A.A., Sale, D.G., Moroz, J.: Comparison of motor unit activation during unilateral and bilateral leg extension. *J. Sport Sci.* **13**, 153–170 (1995)
12. van Ingen Schenau, G.J.: The influence of air friction in speed skating. *J. Biomech.* **15**(6), 449–458 (1982)